APPLIED SCIENCES AND ENGINEERING

Coalescence-induced jumping of droplets on superomniphobic surfaces with macrotexture

Hamed Vahabi[1]*, Wei Wang[1]*, Joseph M. Mabry[2], Arun K. Kota[1,3,4†]

When two liquid droplets coalesce on a superrepellent surface, the excess surface energy is partly converted to upward kinetic energy, and the coalesced droplet jumps away from the surface. However, the efficiency of this energy conversion is very low. In this work, we used a simple and passive technique consisting of superomniphobic surfaces with a macrotexture (comparable to the droplet size) to experimentally demonstrate coalescence-induced jumping with an energy conversion efficiency of 18.8% (i.e., about 570% increase compared to superomniphobic surfaces without a macrotexture). The higher energy conversion efficiency arises primarily from the effective redirection of in-plane velocity vectors to out-of-plane velocity vectors by the macrotexture. Using this higher energy conversion efficiency, we demonstrated coalescence-induced jumping of droplets with low surface tension (26.6 mN m^{-1}) and very high viscosity (220 mPa·s). These results constitute the first-ever demonstration of coalescence-induced jumping of droplets at Ohnesorge number >1.

INTRODUCTION

When two liquid droplets coalesce, the overall surface area of the merged droplet reduces, which results in a release of the excess surface energy. When this droplet coalescence occurs on a superrepellent surface (i.e., a surface that is extremely repellent to and displays negligible adhesion with the contacting liquid), the released excess surface energy is partly converted into the out-of-plane kinetic energy (due to symmetry breaking), allowing the coalesced droplet to jump away from the superrepellent surface (*1*–*17*). Previous work on coalescence-induced jumping has demonstrated that the efficiency η of converting the excess surface energy to the out-of-plane kinetic energy (which causes the droplet to jump away from the surface) is very low (*2*–*7*). This low energy conversion efficiency does not allow coalescence-induced jumping of high-viscosity droplets (due to substantial viscous dissipation) or low–surface tension droplets (due to lack of sufficient excess surface energy) (*7*, *18*). To enable the coalescence-induced jumping of a wide range of liquids (including those with high viscosity or low surface tension), it is necessary to increase the energy conversion efficiency. However, to the best of our knowledge, there are no reports of simple and passive techniques that can increase the energy conversion efficiency in coalescence-induced jumping on superrepellent surfaces (*19*–*24*). In this work, we used superomniphobic surfaces (i.e., surfaces that are repellent to virtually any liquid) (*25*–*30*) having a protruding macrotexture (comparable to the droplet size) to experimentally demonstrate coalescence-induced jumping with energy conversion efficiency η ≈ 18.8% (i.e., about 570% increase in energy conversion efficiency compared to superomniphobic surfaces without a macrotexture). Our numerical simulations indicate that the increase in energy conversion efficiency arises primarily from the effective redirection of in-plane velocity vectors to out-of-plane velocity vectors due to the presence of the protruding macrotexture. Using the substantial increase in energy conversion efficiency on our superomniphobic surfaces with a macrotexture, we demonstrate the coalescence-induced jumping of low–surface tension droplets (e.g., *n*-tetradecane with surface tension $\gamma_{lv} \approx 26.6$ mN m^{-1} and viscosity $\mu \approx 2.1$ mPa·s) and very high–viscosity droplets (e.g., water + 90% glycerol with $\gamma_{lv} \approx 64$ mN m^{-1} and $\mu \approx 220$ mPa·s) (*31*). This is the first-ever demonstration of coalescence-induced jumping at Ohnesorge number Oh > 1 (*32*). Furthermore, based on a nondimensionalized energy balance that accounts for the additional surface energy stored in the coalesced droplet due to the presence of the protruding macrotexture, we demonstrate that the Weber number at droplet departure (a measure of the conversion of surface energy into upward kinetic energy) increases linearly with the nondimensional macrotexture height. We envision that the results and insights obtained from our work will affect a wide variety of applications including self-cleaning, anti-icing, energy harvesting, hot spot cooling, condensation, and lab-on-chip devices, especially when liquids with significant viscous dissipation and/or systems with significant solid-liquid adhesion are involved (*9*, *11*–*17*, *23*, *33*).

RESULTS AND DISCUSSION

To investigate the influence of the protruding macrotexture, we experimentally and numerically (see Materials and methods and sections S1 and S2) studied the coalescence of two water droplets (density $\rho \approx 1000$ kg m^{-3}, $\mu \approx 1$ mPa·s, $\gamma_{lv} \approx 72$ mN m^{-1}, and $R_0 \approx 600$ μm) placed with a micropipette on superomniphobic surfaces without and with a protruding macrotexture (a triangular ridge; see Fig. 1A). Both our experimental results (see Fig. 1, B and D) and numerical results (see Fig. 1, C and E) indicate ~570% increase in out-of-plane kinetic energy of the coalesced droplet on superomniphobic surfaces with the ridge compared to those without the ridge (also see movies S1 and S2). This manifests as a substantial increase in the jumping velocity and jumping height of the droplets on superomniphobic surfaces with the ridge. In Fig. 1 (B to E), please note that the series of six images (from left to right) represents the following physical events: (i) onset of coalescence, (ii) capillary bridge impinging the surface, (iii) maximum contraction of the coalesced droplet, (iv) departure of the coalesced droplet from the surface, (v) maximum height attained by the coalesced droplet after departing from the surface, and (vi) coalesced droplet impacting the surface upon return.

To understand the physical principles underlying this increase in out-of-plane kinetic energy, we numerically studied the evolution of the excess surface energy (i.e., driving force of coalescence) and the

[1]Department of Mechanical Engineering, Colorado State University, Fort Collins, CO 80523, USA. [2]Rocket Propulsion Division, Air Force Research Laboratory, Edwards AFB, CA 93524, USA. [3]School of Biomedical Engineering, Colorado State University, Fort Collins, CO 80523, USA. [4]Department of Chemical Engineering, Colorado State University, Fort Collins, CO 80523 USA.
*These authors contributed equally to this work.
†Corresponding author. Email: arun.kota@colostate.edu

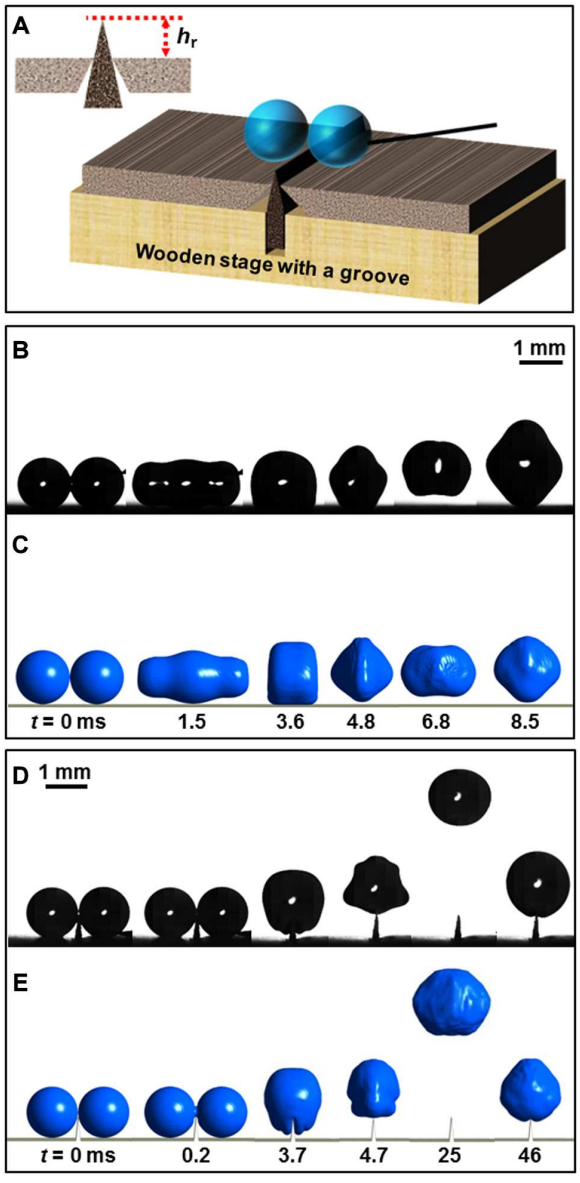

Fig. 1. Coalescence-induced self-propulsion with and without a ridge. (**A**) Schematic of the experimental setup used to study the coalescence-induced self-propulsion of liquid droplets. The inset shows the ridge height h_r. A series of snapshots showing the coalescence-induced self-propulsion of water droplets ($R_0 \approx 600$ μm) on superomniphobic surfaces (**B**) without a ridge (experimental), (**C**) without a ridge (numerical), (**D**) with a ridge (experimental), and (**E**) with a ridge (numerical). In (D) and (E), the ridge height $h_r \approx 500$ μm. Time difference between the experimental snapshots and the corresponding numerical snapshots is <0.2 ms (also see movies S1 and S2).

upward kinetic energy (i.e., kinetic energy by virtue of the net upward velocity) during coalescence of droplets on a superomniphobic surface without and with a ridge. We define the coordinate system as follows—droplets coalesce along the x direction, the ridge is along the y direction, and the coalesced droplet jumps along the z direction (see inset in Fig. 2A and section S2). The onset of coalescence of droplets with R_0 occurs at time $t = 0$, and eventually, the coalesced droplet attains a radius $R_c \approx 2^{1/3}R_0$. At any time t during the coalescence, the driving force for coalescence is the excess surface energy $E_{surf,ex}(t) = E_{surf}(t) - E_{surf,c}$, where $E_{surf}(t) = \gamma_{lv}A_{surf}(t)$ is the surface energy of droplet, $A_{surf}(t)$ is the surface area of the droplet, and $E_{surf,c} = \gamma_{lv}4\pi R_c^2$ is the surface energy of the coalesced droplet that has eventually attained the R_c. At the onset of coalescence (i.e., $t = 0$), the total available excess surface energy $E_{surf,ex}(0) = E_{surf}(0) - E_{surf,c}$. Here, $E_{surf}(0) = \gamma_{lv}8\pi R_0^2$. During coalescence, this excess surface energy is gradually released. A fraction of the released surface energy is converted to upward kinetic energy $E_{kin,up}(t) = m_c V_{up}^2(t)/2$, where $m_c = \rho 4\pi R_c^3/3$ is the mass of the coalesced droplet and $V_{up}(t)$ is the net upward velocity of the coalesced droplet (see section S3). In our analysis, we nondimensionalized the relevant parameters as follows: nondimensional time $t^* = t/t_{ic}$, where $t_{ic} = \sqrt{\rho R_0^3/\gamma_{lv}}$ is the inertial-capillary time scale, the nondimensional excess surface energy $E^*_{surf,ex}(t^*) = E_{surf,ex}(t)/E_{surf,ex}(0)$, and the nondimensional upward kinetic energy $E^*_{kin,up}(t^*) = E_{kin,up}(t)/E_{surf,ex}(0)$. At the onset of coalescence (i.e., at $t^* = 0$), $E^*_{surf,ex}(0) = 1$ and $E^*_{kin,up}(0) = 0$. When the droplet departs from the surface at $t = t_d$ (i.e., at $t^* = t^*_d$), the energy conversion efficiency $\eta = E^*_{kin,up}(t^*_d)$. To better explain the physical phenomena, we classify coalescence into three stages: Stage I is from the onset of coalescence until the capillary bridge impinges on the surface, stage II is from the capillary bridge impinging on the surface until the maximum solid-liquid contact area is attained, and stage III is from the maximum solid-liquid contact area until the droplet departs from the surface, as described in more detail below.

First, let us consider two droplets of water ($R_0 \approx 600$ μm) coalescing on a superomniphobic surface without a ridge (see Fig. 2A and movie S3). Upon coalescence, the capillary bridge begins to expand in y and z directions, the excess surface energy $E^*_{surf,ex}(t^*)$ reduces with time t^*, and because of the symmetric deformation of the droplet relative to the xy plane of coalescence, the net upward velocity of the droplet $V_{up} = 0$ and the upward kinetic energy of the droplet $E^*_{kin,up} = 0$ (see stage I in Fig. 2A and section S4). At $t^* \approx 1$ (i.e., $t \approx t_{ic}$) (*3*, *5*, *7*), the capillary bridge impinges on the superomniphobic surface (see Fig. 2B and section S5), causing symmetry breaking, which forces the droplet (i.e., the center of mass) to move upward, resulting in a net upward velocity V_{up} (*3*, *5*, *7*) and upward kinetic energy of the droplet $E^*_{kin,up}$ (see stage II in Fig. 2A). Simultaneously, the droplet displays maximum expansion in the x direction with two symmetric, high-pressure lobes at $+x$ and $-x$ extremes (see Fig. 2C and section S5). Subsequently, the internal flow from the high-pressure regions at the lobes to the low-pressure region near the center of the droplet results in droplet contraction in the x direction, with maximum contraction and maximum solid-liquid contact area at $t^* \approx 2$ (see Fig. 2D and section S5) (*3*, *5*, *7*). The maximum contraction results in a high-pressure region near the center of the droplet, and the maximum contact area results in the maximum upward reaction force on the droplet (*3*, *5*, *7*). This upward reaction force aligns the velocity vectors in the $+z$ direction, resulting in further increase in the upward kinetic energy of the droplet $E^*_{kin,up}$ (see stage III in Fig. 2A). However, the radially outward internal flow from the high-pressure region near the center of the droplet disturbs the alignment of velocity vectors (see Fig. 2E and section S5), impeding the upward motion of the droplet. Consequently, when the droplet departs from the superomniphobic surface at $t^* = t^*_d$ (see Fig. 2F and section S5), it does so with a relatively low upward kinetic energy and a relatively low energy conversion efficiency $\eta = E^*_{kin,up}(t^*_d) \approx 2.8\%$ (see stage III in Fig. 2A) (*2*, *3*, *5*).

Now, let us consider two similar droplets of water ($R_0 \approx 600$ μm) coalescing on a superomniphobic surface with a ridge (ridge height $h_r \approx 500$ μm; see Fig. 3A and movie S3). Upon coalescence, similar to that

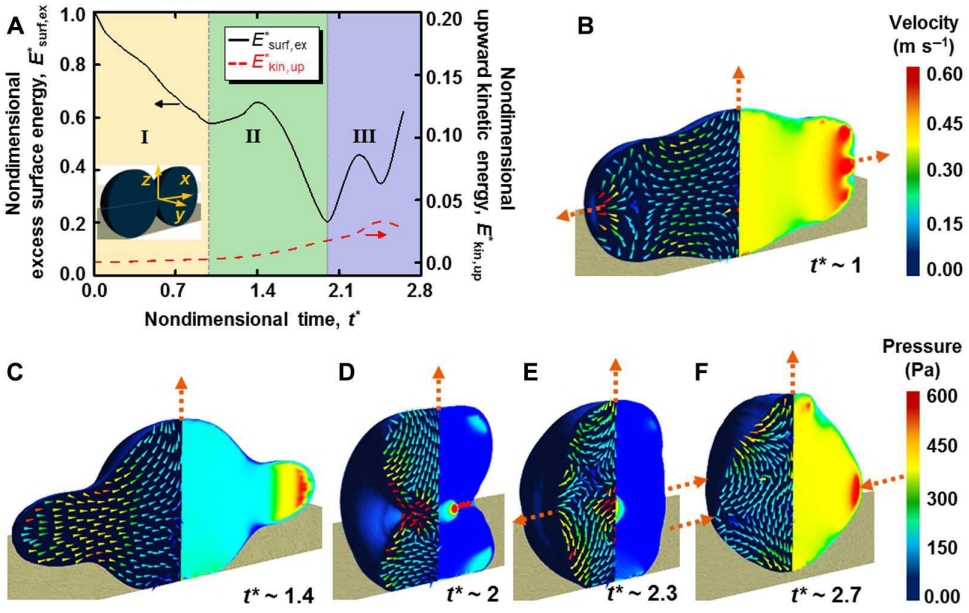

Fig. 2. Droplet dynamics without a ridge. (**A**) Evolution of the nondimensional excess surface energy ($E^*_{surf,ex}$) and the nondimensional upward kinetic energy ($E^*_{kin,up}$) during the coalescence of water droplets ($R_0 \approx 600$ μm) on a superomniphobic surface without a ridge. The inset shows the coordinate system. The three stages (I, II, and III) of coalescence are shown with different colors. (**B** to **F**) A series of snapshots showing the pressure distribution and velocity vectors within the droplet on a superomniphobic surface without a ridge. The colors represent the magnitude of pressure and velocity. The dotted orange arrows at droplet periphery indicate the direction of droplet deformation (also see movie S3).

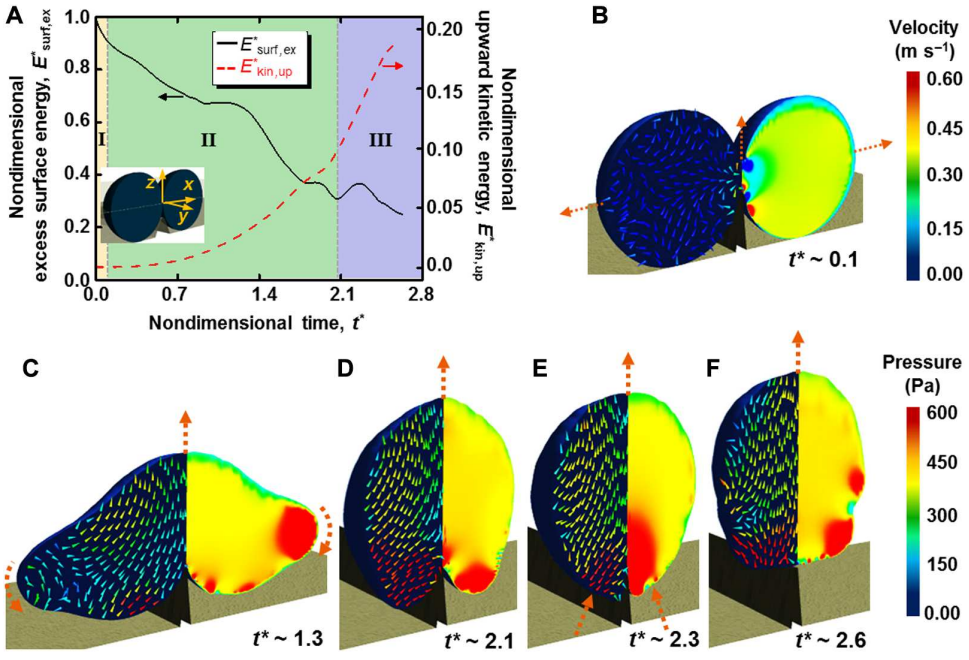

Fig. 3. Droplet dynamics with a ridge. (**A**) Evolution of the nondimensional excess surface energy ($E^*_{surf,ex}$) and the nondimensional upward kinetic energy ($E^*_{kin,up}$) during the coalescence of water droplets ($R_0 \approx 600$ μm) on a superomniphobic surface with a ridge (ridge height $h_r \approx 500$ μm). The inset shows the coordinate system. The three stages (I, II, and III) of coalescence are shown with different colors. (**B** to **F**) A series of snapshots showing the pressure distribution and velocity vectors within the droplet on a superomniphobic surface with a ridge. The colors represent the magnitude of pressure and velocity. The dotted orange arrows at droplet periphery indicate the direction of droplet deformation (also see movie S3).

on a superomniphobic surface with no ridge, the capillary bridge begins to expand in y and z directions, the excess surface energy $E^*_{surf,ex}(t^*)$ reduces with time t^*, and because of the symmetric deformation of the droplet relative to the xy plane of coalescence, the net upward velocity of the droplet $V_{up} = 0$ and the upward kinetic energy of the droplet $E^*_{kin,up} = 0$ (see stage I in Fig. 3A). As might be anticipated, in contrast to the superomniphobic surface with no ridge, the presence of the ridge forces the capillary bridge to impinge on the superomniphobic surface at

$t^* < 1$ (i.e., $t < t_{ic}$), causing early symmetry breaking (see Fig. 3B and section S5). Subsequently, similar to that on a superomniphobic surface with no ridge, the symmetry breaking forces the droplet (i.e., the center of mass) to move upward, resulting in a net upward velocity V_{up} and upward kinetic energy $E^*_{kin,up}$ (see stage II in Fig. 3A). Simultaneously, the droplet displays maximum expansion in the x direction with two symmetric, high-pressure lobes at $+x$ and $-x$ extremes (see Fig. 3C and section S5). Subsequently, the internal flow from the high-pressure regions at the lobes to the low-pressure region near the center of the droplet results in the onset of droplet contraction in the x direction. However, in notable contrast to the superomniphobic surface with no ridge, during droplet contraction in the x direction, the obstruction posed by the ridge redirects the velocity vectors primarily in the $+z$ direction (see Fig. 3D and section S5). This redirection of the velocity vectors results in a significant increase in the $E^*_{kin,up}$ (see stage II in Fig. 3A). Simultaneously, the high-pressure regions move downward (i.e., $-z$ direction), and the droplet "wraps" around the ridge with maximum solid-liquid contact area at $t^* \approx 2.1$ (see Fig. 3D). The maximum contact area results in maximum upward reaction force. A combination of the upward reaction force and the high-pressure regions at the bottom of the droplet (unlike the high-pressure region near the center of the droplet for coalescence on a superomniphobic surface with no ridge) synergistically leads to further alignment of velocity vectors in the $+z$ direction (see Fig. 3E and section S5), resulting in further increase in the upward kinetic energy of the droplet $E^*_{kin,up}$ (see stage III in Fig. 3A). Consequently, when the droplet departs from the superomniphobic surface with the ridge at $t^* = t^*_d$ (see Fig. 3F and section S5), it does so with a high upward kinetic energy and a high energy conversion efficiency $\eta = E^*_{kin,up}(t^*_d) \approx 18.8\%$ (see stage III in Fig. 3A). This high energy conversion efficiency η is also possible in coalescence of significantly smaller droplets ($R_0 << 600$ μm) with ridges comparable to droplet size (see section S6).

It is evident from the preceding discussion that the energy conversion efficiency during coalescence on a superomniphobic surface with a ridge is ~570% higher than that on a superomniphobic surface without a ridge (see Figs. 2A and 3A). The higher energy conversion efficiency arises primarily from the effective redirection of in-plane velocity vectors to out-of-plane velocity vectors by the ridge. Using this high energy conversion efficiency, we can now achieve coalescence-induced jumping of low–surface tension droplets (e.g., n-tetradecane with $\rho \approx 760$ kg m^{-3}, $\mu \approx 2.1$ mPa·s, $\gamma_{lv} \approx 26.6$ mN m^{-1}, and $R_0 \approx 480$ μm; see Fig. 4, A and B, and movie S4) and high-viscosity droplets (e.g., water + 90% glycerol with $\rho \approx 1230$ kg m^{-3}, $\mu \approx 220$ mPa·s, $\gamma_{lv} \approx 64$ mN m^{-1}, and $R_0 \approx 480$ μm; see Fig. 4, C and D, and movie S5) (*31*) on superomniphobic surfaces with a ridge. Note that we did not observe coalescence-induced jumping of these low–surface tension and high-viscosity droplets on superomniphobic surfaces without a ridge (see section S7 and movie S6). Further, for our coalescence-induced jumping of water + 90% glycerol droplets on superomniphobic surfaces with a ridge, the Ohnesorge number $Oh = \mu/\sqrt{\rho\gamma_{lv}R_0} \approx 1.14$. To the best of our knowledge, this is the first-ever demonstration of coalescence-induced jumping of droplets at $Oh > 1$, i.e., in the viscosity-dominated regime (*3*–*7*).

To quantitatively investigate the influence of ridge height h_r on the coalescence-induced jumping velocity V_j [note that $V_j = V_{up}(t_d)$], we numerically investigated the coalescence-induced jumping of water droplets with different radii (R_0 = 60, 180, and 600 μm) on superomniphobic surfaces with ridges of different heights ($0 < h_r < 600$ μm). Our results (Fig. 5A) indicate that the jumping velocity V_j increases with increasing ridge height h_r and decreasing R_0. To physically understand these trends, we rely on scaling arguments based on an energy balance. During droplet coalescence in the inertial-capillary regime on a superomniphobic surface without a ridge, excess surface energy is partly converted to the upward kinetic energy of the droplet. The corresponding scaling argument based on an energy balance can be written as (*2*–*7*, *24*)

$$\rho R_0^3 V_j^2 \sim \gamma_{lv} R_0^2 \tag{1}$$

Similarly, during droplet coalescence in the inertial-capillary regime on a superomniphobic surface with a ridge, excess surface energy is partly converted to the upward kinetic energy of the droplet. However, in notable contrast to the superomniphobic surface without a ridge, during coalescence on a superomniphobic surface with a ridge, the droplet wraps around the ridge (see Fig. 3D). In this configuration, additional surface energy is stored in the deformed droplet. This additional surface energy scales as $\gamma_{lv}R_0h_r$. When the droplet departs from the surface (i.e., $t = t_d$), in addition to the excess surface energy, this additional surface energy stored in the deformed droplet is partly converted to upward kinetic energy. The corresponding scaling argument based on an energy balance can be written as

$$\rho R_0^3 V_j^2 \approx C_1 \gamma_{lv} R_0^2 + C_2 \gamma_{lv} R_0 h_r \tag{2}$$

Here, the constants C_1 and C_2 account for the partial energy conversion and the geometric factors. Nondimensionalizing the ridge height as $h^* = h_r/R_0$ and the jumping velocity as $V_j^* = V_j/V_{ic}$, where $V_{ic} = \sqrt{\gamma_{lv}/\rho R_0}$ is the inertial-capillary velocity, Eq. 2 can be rewritten as

$$We_j \sim C_1 + C_2 h^* \tag{3}$$

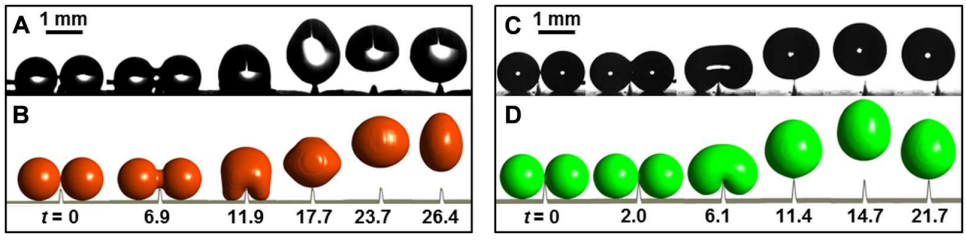

Fig. 4. Coalescence-induced self-propulsion of low–surface tension and high-viscosity droplets. A series of snapshots showing the coalescence-induced self-propulsion of n-tetradecane droplets ($R_0 \approx 480$ μm and $\gamma_{lv} \approx 26.6$ mN m^{-1}) on a superomniphobic surface with a ridge— (**A**) experimental and (**B**) numerical (also see movie S4). A series of snapshots showing the coalescence-induced self-propulsion of water + 90% glycerol droplets ($R_0 \approx 480$ μm and $\mu \approx 220$ mPa·s) on a superomniphobic surface with a ridge—(**C**) experimental and (**D**) numerical (also see movie S5).

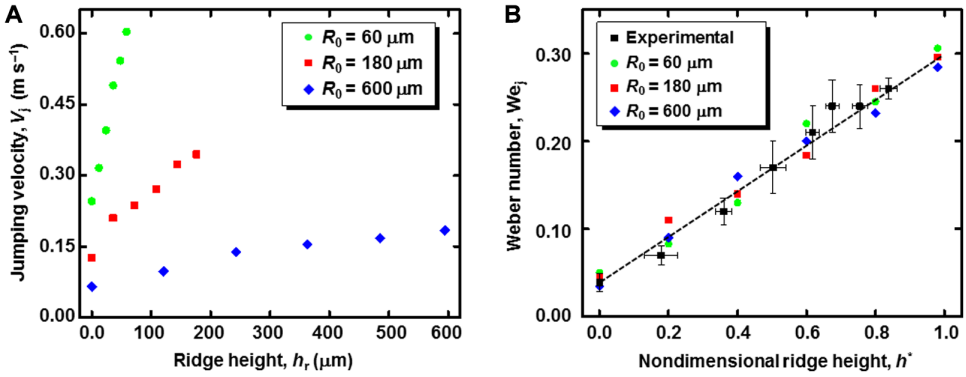

Fig. 5. Jumping velocity of coalescing droplets with and without a ridge. (**A**) Jumping velocity of droplets with different radii on superomniphobic surfaces with different ridge heights (data from numerical simulations). (**B**) Both numerical and experimental data collapse onto a single nondimensional straight line of Weber number at droplet departure (or jumping) versus nondimensional ridge height, in accordance with Eq. 3. Error bars in the experimental data represent the error associated with velocity, droplet radius, and ridge height measurements.

Here, $We_j = V_j^{*2} = \rho R_0 V_j^2/\gamma_{1v}$ is the Weber number when the droplet departs (or jumps away) from the surface. We_j is a measure of the conversion of surface energy into upward kinetic energy (see section S8). It is evident from Eq. 3 that We_j increases linearly with increasing nondimensional ridge height h^*. Physically, this implies that a higher h_r or a smaller droplet R_0 leads to a more efficient conversion of the surface energy to upward kinetic energy. Both our numerical and experimental results (with different R_0 and h_r) collapse onto a single nondimensional straight line in accordance with Eq. 3, confirming the validity of our scaling arguments (see Fig. 5B). It is evident that at $h^* = 0$ (i.e., on a superomniphobic surface without a ridge), $We_j = V_j^{*2} \approx 0.041$ (i.e., nondimensional jumping velocity, $V_j^* \approx 0.2$), which is in good agreement with previous reports of coalescence-induced jumping on superrepellent surfaces without a ridge (*2*–*7*, *24*).

CONCLUSION

In summary, we used a simple and passive technique consisting of superomniphobic surfaces with a ridge to experimentally demonstrate coalescence-induced jumping with a high energy conversion efficiency $\eta \approx 18.8\%$ (i.e., about 570% increase in energy conversion efficiency compared to superomniphobic surfaces without a ridge). Using the significant increase in energy conversion efficiency on our superomniphobic surfaces with a ridge, we demonstrate the coalescence-induced jumping of low–surface tension droplets (e.g., *n*-tetradecane with $\gamma_{lv} \approx 26.6$ mN m^{-1}) and very high–viscosity droplets (e.g., water + 90% glycerol with $\mu \approx 220$ mPa·s). These results constitute the first-ever demonstration of coalescence-induced jumping of droplets at Oh > 1, i.e., in the viscosity-dominated regime. We envision that the results and insights obtained from our work will affect a wide variety of applications including self-cleaning, anti-icing, energy harvesting, hot spot cooling, condensation, and lab-on-chip devices, especially when liquids with substantial viscous dissipation and/or systems with significant solid-liquid adhesion are involved (*9*, *11*–*17*, *23*, *33*). Specifically, we anticipate that superrepellent surfaces that have hierarchically structured, periodic ridges throughout the surface can enhance the energy conversion efficiency in practical applications with droplet coalescence at multiple length scales (see section S9) (*34*, *35*).

Further, our numerical simulations indicate that the underlying mechanism for the increase in energy conversion efficiency is the effective redirection of in-plane velocity vectors to out-of-plane velocity vectors due to the presence of the ridge. Based on a nondimensionalized energy balance that accounts for the additional surface energy stored in the coalesced droplet due to the presence of the ridge, we demonstrated that the Weber number at droplet departure (a measure of the conversion of surface energy into upward kinetic energy) increases linearly with the nondimensional ridge height. In this context, it is interesting to note that protruding macrotextures on superrepellent surfaces can favorably alter the droplet dynamics in coalescence (by increasing the jumping velocity and energy conversion efficiency) and in bouncing or splitting (by reducing the contact time) (*36*, *37*) to enhance the departure of the droplet from the surface. In droplet coalescence on macrotextures, surface energy is converted to kinetic energy, and in droplet bouncing or splitting on macrotextures, kinetic energy is converted to surface energy; in both cases, some energy is lost to viscous dissipation. The scaling arguments presented in our work, especially those related to surface energy stored in a deformed droplet, may be useful to understand droplet dynamics in bouncing and splitting on ridges. While our work has primarily focused on incorporating the influence of the ridge height into the scaling arguments, a more detailed study is necessary to incorporate the influence of the ridge angle into the scaling arguments (see section S10).

MATERIALS AND METHODS

Fabrication of superomniphobic surfaces

A solution (20 mg/ml) of 20 weight % (wt %) SF100 (super fast instant adhesive3M) + 80 wt % fluorodecyl polyhedral oligomeric silsesquioxanes (POSS) (*38*) in ASAHIKLIN AK-225 (Asahi Glass) was spray coated (at a pressure of ≈ 200 kPa) onto the desired surface using an air brush (Paasche) held 15 cm from the surface. Subsequently, the substrate was allowed to dry at room temperature for an hour. Our surfaces were superomniphobic for liquids with a wide range of surface tensions ($\gamma_{lv} \geq 25.3$ mN m^{-1}).

Coalescence experiments

An experimental apparatus composed of three pieces (i.e., a ridge and two flat solid surfaces) mounted on a wooden stage with a groove (see Fig. 1A) was used to study the coalescence-induced jumping of liquid droplets. The ridge was fabricated by machining an as-received 6061 aluminum sheet (thickness ≈ 0.4 mm; McMaster-Carr) with a bench-top grinding machine. The ridge was then placed between two

flat aluminum sheets (2 cm by 2 cm) with beveled edges. By adjusting the location of the ridge within the wooden groove, we altered the height of the ridge (100 μm < h_r < 500 μm). After spray coating the ridge and the two flat sheets with 20 wt % SF100 + 80 wt % fluorodecyl POSS blends (see the "Fabrication of superomniphobic surfaces" section), two droplets of equal volume (dispensed with a micropipette) were placed on either side of the ridge. A very thin metal fiber (also spray coated with a superomniphobic coating) was used as a maneuvering probe to gently nudge one of the droplets (with negligible horizontal velocity) and induce coalescence. Note that a thinner coating of 20 wt % SF100 + 80 wt % fluorodecyl POSS blends was sufficient to obtain superrepellency for high–surface tension liquids (e.g., water and water + 90% glycerol), but a thicker coating, especially at the tip of the ridge (to ensure multiple layers of reentrant texture), was necessary to obtain superrepellency for low–surface tension liquids. Consequently, the ridges used for coalescence of high–surface tension liquid droplets were sharper (ridge angle α ≈ 15°; see Figs. 1D and 4C), and the ridges used for coalescence of low–surface tension liquid droplets were blunter (ridge angle α ≈ 25°; see Fig. 4A).

High-speed imaging

High-speed movies of coalescing droplets were obtained using a high-speed camera (Photron FASTCAM SA3) at 3000 frames/s. We determined the jumping velocity of the coalesced droplet from the droplet trajectories, as explained in our previous work (*7*). Some droplets deviated from the vertical direction during jumping because of the mismatch in droplets sizes, asymmetry in the geometry of the ridge, and asymmetry in coalescence. Thus, we restricted all our experimental analyses to jumping droplets within a deviation of ±10° from the vertical direction.

Contact angle and roll-off angle measurements

A contact angle goniometer (Ramé-Hart 260) was used to measure the apparent contact angles and roll-off angles using ≈ 5 μl of droplets. The contact angles were measured by advancing or receding the droplets on the surface using a syringe (Gilmont). The roll-off angles were measured by tilting the stage until the droplet rolled off from the surface. At least six measurements were performed on each surface. The errors in contact angle and roll-off angle measurements were ±2° and ±1°, respectively. The apparent advancing contact angle θ^*_{adv}, the apparent receding contact angle θ^*_{rec}, and the roll-off angle ω of the liquids used in this study are listed in section S1.

Morphology characterization

Morphology of the spray-coated surfaces and the ridge angles after spray coating were characterized using a scanning electron microscope (JEOL 6500F) at 5 kV (section S1).

Numerical simulations

We implemented three-dimensional numerical simulations with an incompressible, laminar flow model to capture the evolution of the liquid-air interface during the coalescence of two identical liquid droplets (R_0) resting on a superomniphobic surface. Similar to previous studies (*2*, *3*, *5*, *7*, *39*, *40*), we used smooth surfaces (with perfectly smooth wall boundary conditions), with known contact angles [i.e., $\theta^* \approx (\theta^*_{adv} + \theta^*_{rec})/2$; see table S1], to define the superomniphobic surfaces in our numerical simulations. Since the experimentally measured contact angle hysteresis is low (i.e., $\Delta\theta^* < 10°$; see table S1) on our superomniphobic surfaces, in our numerical simulations, we ignored contact angle hysteresis at the superomniphobic ridge and at the lower boundary of the computational domain (i.e., $z = 0$; see section S2) representing the flat superomniphobic surfaces. The two droplets were initially situated with overlapping diffuse interfaces that led to the onset of coalescence (*3*, *5*, *7*). Because of the symmetry in the x and y directions, only half of a coalescing droplet was simulated in a computational domain of $6R_0 \times 6R_0 \times 10R_0$ (see section S2) (*3*, *5*, *7*). Symmetric boundary conditions were used at the planes $x = 0$ and $y = 0$ (*5*, *7*). We solved the governing equations (equation of continuity and momentum equation) with ANSYS Fluent using a pressure-based solver (*7*). The geometric reconstruction scheme was used in the volume of fluid model to represent the liquid-air interface, with a piecewise-linear approach. Further, we used the continuum surface force method, with surface tension as the source term in the momentum equation. The momentum equation was discretized using the second-order upwind scheme (*7*). We used the SIMPLE (semi implicit-explicit) algorithm for pressure-velocity coupling, and fluid properties were updated from the pressures using the PISO (pressure implicit with splitting of operators) algorithm (*7*). A mesh with >40 cells per radius was used within the droplet (*7*). Further, local mesh refinement was performed close to the ridge, the lower boundary of the computational domain (i.e., $z \to 0$), and the symmetry planes (i.e., $x \to 0$ and $y \to 0$) to mitigate the influence of high gradients (see section S2). A mesh-independence check was performed to confirm that the numerical results were virtually insensitive to further mesh refinement. A variable time-step scheme was used in all cases to ensure Courant-Friedrich-Levy number < 0.8 in each time step. Iterations at each time step were terminated when the convergence criteria of all equations was smaller than 10^{-6}.

SUPPLEMENTARY MATERIALS

Supplementary material for this article is available at http://advances.sciencemag.org/cgi/content/full/4/11/eaau3488/DC1

Supplementary Text

Fig. S1. Morphology of the superomniphobic ridge.

Fig. S2. Computational domain.

Fig. S3. Components of the total kinetic energy.

Fig. S4. Velocity vectors and pressure distribution (*yz* view).

Fig. S5. Coalescence-induced jumping of smaller droplets.

Fig. S6. Coalescence of low–surface tension and high-viscosity droplets.

Fig. S7. Schematic of a superrepellent surface with periodic arrangement of triangular ridges.

Fig. S8. Schematic of two coalescing droplets and a ridge with maximum ridge angle.

Fig. S9. Schematic depicting the influence of nondimensional ridge height h^* on the maximum ridge angle α_{max}.

Table S1. Density, viscosity, surface tension, apparent advancing contact angle, apparent receding contact angle, and roll-off angle of test liquids on superomniphobic surfaces.

Table S2. Influence of the ridge angle α on the energy conversion efficiency η in coalescence-induced jumping of droplets with radius R_0 = 600 μm at different nondimensional ridge heights h^*.

Movie S1. This video illustrates (experimentally and numerically) the coalescence-induced self-propulsion of two droplets of water (R_0 ≈ 600 μm) on a superomniphobic surface without a ridge.

Movie S2. This video illustrates (experimentally and numerically) the coalescence-induced self-propulsion of two droplets of water (R_0 ≈ 600 μm) on a superomniphobic surface with a ridge (ridge height h_r ≈ 500 μm).

Movie S3. This video illustrates the evolution of the velocity vectors within two droplets of water (R_0 ≈ 600 μm) during their coalescence on a superomniphobic surface with and without a ridge.

Movie S4. This video illustrates (experimentally and numerically) the coalescence-induced self-propulsion of two droplets (R_0 ≈ 480 μm) of a low–surface tension liquid (*n*-tetradecane with γ_{lv} ≈ 26.6 mN m^{-1}) on a superomniphobic surface with a ridge.

Movie S5. This video illustrates (experimentally and numerically) the coalescence-induced self-propulsion of two droplets (R_0 ≈ 480 μm) of a high-viscosity liquid (water + 90% glycerol with μ ≈ 220 mPa·s) on a superomniphobic surface with a ridge.

Movie S6. This video illustrates the coalescence of two low–surface tension droplets (*n*-tetradecane with $\gamma_{lv} \approx 26.6$ mN m^{-1} and $R_0 \approx 480$ μm) and two high-viscosity droplets (water + 90% glycerol with $\mu \approx 220$ mPa·s and $R_0 \approx 480$ μm) on a superomniphobic surface without a ridge.

REFERENCES AND NOTES

1. J. B. Boreyko, C.-H. Chen, Self-propelled dropwise condensate on superhydrophobic surfaces. *Phys. Rev. Lett.* **103**, 184501 (2009).
2. R. Enright, N. Miljkovic, J. Sprittles, K. Nolan, R. Mitchell, E. N. Wang, How coalescing droplets jump. *ACS Nano* **8**, 10352–10362 (2014).
3. F. Liu, G. Ghigliotti, J. J. Feng, C.-H. Chen, Numerical simulations of self-propelled jumping upon drop coalescence on non-wetting surfaces. *J. Fluid Mech.* **752**, 39–65 (2014).
4. F. Liu, G. Ghigliotti, J. J. Feng, C.-H. Chen, Self-propelled jumping upon drop coalescence on Leidenfrost surfaces. *J. Fluid Mech.* **752**, 22–38 (2014).
5. Y. Cheng, J. Xu, Y. Sui, Numerical investigation of coalescence-induced droplet jumping on superhydrophobic surfaces for efficient dropwise condensation heat transfer. *Int. J. Heat Mass Transfer* **95**, 506–516 (2016).
6. H. Cha, C. Xu, J. Sotelo, J. M. Chun, Y. Yokoyama, R. Enright, N. Miljkovic, Coalescence-induced nanodroplet jumping. *Phys. Rev. Fluids* **1**, 064102 (2016).
7. H. Vahabi, W. Wang, S. Davies, J. M. Mabry, A. K. Kota, Coalescence-induced self-propulsion of droplets on superomniphobic surfaces. *ACS Appl. Mater. Interfaces* **9**, 29328–29336 (2017).
8. T. Mouterde, T.-V. Nguyen, H. Takahashi, C. Clanet, I. Shimoyama, D. Quéré, How merging droplets jump off a superhydrophobic surface: Measurements and model. *Phys. Rev. Fluids* **2**, 112001 (2017).
9. K. M. Wisdom, J. A. Watson, X. Qu, F. Liu, G. S. Watson, C.-H. Chen, Self-cleaning of superhydrophobic surfaces by self-propelled jumping condensate. *Proc. Natl. Acad. Sci. U.S.A.* **110**, 7992–7997 (2013).
10. J. B. Boreyko, C.-H. Chen, Self-propelled jumping drops on superhydrophobic surfaces. *Phys. Rev. Fluids* **22**, 091110 (2010).
11. K. Rykaczewski, J. H. J. Scott, S. Rajauria, J. Chinn, A. M. Chinnd, W. Jones, Three dimensional aspects of droplet coalescence during dropwise condensation on superhydrophobic surfaces. *Soft Matter* **7**, 8749–8752 (2011).
12. X. Chen, R. S. Patel, J. A. Weibel, S. V. Garimella, Coalescence-induced jumping of multiple condensate droplets on hierarchical superhydrophobic surfaces. *Sci. Rep.* **6**, 18649 (2016).
13. C. Hao, Y. Liu, X. Chen, J. Li, M. Zhang, Y. Zhao, Z. Wang, Bioinspired interfacial materials with enhanced drop mobility: From fundamentals to multifunctional applications. *Small* **12**, 1825–1839 (2016).
14. D. G. Aarts, H. N. Lekkerkerker, H. Guo, G. H. Wegdam, D. Bonn, Hydrodynamics of droplet coalescence. *Phys. Rev. Lett.* **95**, 164503 (2005).
15. N. Miljkovic, R. Enright, Y. Nam, K. Lopez, N. Dou, J. Sack, E. N. Wang, Jumping-droplet-enhanced condensation on scalable superhydrophobic nanostructured surfaces. *Nano Lett.* **13**, 179–187 (2012).
16. J. Oh, P. Birbarah, T. Foulkes, S. L. Yin, M. Rentauskas, J. Neely, R. C. N. Pilawa-Podgurski, N. Miljkovic, Jumping-droplet electronics hot-spot cooling. *Appl. Phys. Lett.* **110**, 123107 (2017).
17. J. B. Boreyko, C. P. Collier, Delayed frost growth on jumping-drop superhydrophobic surfaces. *ACS Nano* **7**, 1618–1627 (2013).
18. K. Rykaczewski, A. T. Paxson, M. Staymates, M. L. Walker, X. Sun, S. Anand, S. Srinivasan, G. H. McKinley, J. Chinn, J. H. J. Scott, K. K. Varanasi, Dropwise condensation of low surface tension fluids on omniphobic surfaces. *Sci. Rep.* **4**, 4158 (2014).
19. M. D. Mulroe, B. R. Srijanto, S. F. Ahmadi, C. P. Collier, J. B. Boreyko, Tuning superhydrophobic nanostructures to enhance jumping-droplet condensation. *ACS Nano* **11**, 8499–8510 (2017).
20. A. Cavalli, D. J. Preston, E. Tio, D. W. Martin, N. Miljkovic, E. N. Wang, F. Blanchette, J. W. M. Bush, Electrically induced drop detachment and ejection. *Phys. Fluids* **28**, 022101 (2016).
21. N. Miljkovic, D. J. Preston, R. Enright, E. N. Wang, Electrostatic charging of jumping droplets. *Nat. Commun.* **4**, 2517 (2013).
22. N. Miljkovic, D. J. Preston, R. Enright, E. N. Wang, Electric-field-enhanced condensation on superhydrophobic nanostructured surfaces. *ACS Nano* **7**, 11043–11054 (2013).
23. N. Miljkovic, D. J. Preston, R. Enright, E. N. Wang, Jumping-droplet electrostatic energy harvesting. *Appl. Phys. Lett.* **105**, 013111 (2014).
24. K. Zhang, F. Liu, A. J. Williams, X. Qu, J. J. Feng, C.-H. Chen, Self-propelled droplet removal from hydrophobic fiber-based coalescers. *Phys. Rev. Lett.* **115**, 074502 (2015).
25. D. Quéré, Wetting and roughness. *Annu. Rev. Mater. Res.* **38**, 71–99 (2008).
26. H. Vahabi, W. Wang, S. Movafaghi, A. K. Kota, Free-standing, flexible, superomniphobic films. *ACS Appl. Mater. Interfaces* **8**, 21962–21967 (2016).
27. W. Wang, J. Salazar, H. Vahabi, A. Joshi-Imre, W. E. Voit, A. K. Kota, Metamorphic superomniphobic surfaces. *Adv. Mater.* **29**, 1700295 (2017).
28. R. Tadmor, R. Das, S. Gulec, J. Liu, H. E. N'guessan, M. Shah, P. S. Wasnik, S. B. Yadav, Solid–liquid work of adhesion. *Langmuir* **33**, 3594–3600 (2017).
29. H. Vahabi, W. Wang, K. C. Popat, G. Kwon, T. B. Holland, A. K. Kota, Metallic superhydrophobic surfaces via thermal sensitization. *Appl. Phys. Lett.* **110**, 251602 (2017).
30. S. Movafaghi, W. Wang, A. Metzger, D. D. Williams, J. D. Williams, A. K. Kota, Tunable superomniphobic surfaces for sorting droplets by surface tension. *Lab Chip* **16**, 3204–3209 (2016).
31. J. B. Segur, H. E. Oberstar, Viscosity of glycerol and its aqueous solutions. *Ind. Eng. Chem. Res.* **43**, 2117–2120 (1951).
32. G. H. McKinley, M. Renardy, Wolfgang von Ohnesorge. *Phys. Fluids* **23**, 127101 (2011).
33. X. Chen, J. Wu, R. Ma, M. Hua, N. Koratkar, S. Yao, Z. Wang, Nanograssed micropyramidal architectures for continuous dropwise condensation. *Adv. Funct. Mater.* **21**, 4617–4623 (2011).
34. X. Qu, J. B. Boreyko, F. Liu, R. L. Agapov, N. V. Lavrik, S. T. Retterer, J. J. Feng, C. P. Collier, C.-H. Chen, Self-propelled sweeping removal of dropwise condensate. *Appl. Phys. Lett.* **106**, 221601 (2015).
35. B. K. Chakraverty, G. Pound, Heterogeneous nucleation at macroscopic steps. *Acta Metall.* **12**, 851–860 (1964).
36. J. C. Bird, R. Dhiman, H.-M. Kwon, K. K. Varanasi, Reducing the contact time of a bouncing drop. *Nature* **503**, 385–388 (2013).
37. A. Gauthier, S. Symon, C. Clanet, D. Quéré, Water impacting on superhydrophobic macrotextures. *Nat. Commun.* **6**, 8001 (2015).
38. J. M. Mabry, A. Vij, S. T. Iacono, B. D. Viers, Innentitelbild: Fluorinated polyhedral oligomeric silsesquioxanes (F-POSS). *Angew. Chem.* **120**, 4094 (2008).
39. Y. Nam, H. Kim, S. Shin, Energy and hydrodynamic analyses of coalescence-induced jumping droplets. *Appl. Phys. Lett.* **103**, 161601 (2013).
40. F. C. Wang, F. Yang, Y. P. Zhao, Size effect on the coalescence-induced self-propelled droplet. *Appl. Phys. Lett.* **98**, 053112 (2011).

Acknowledgments

Funding: A.K.K. acknowledges financial support under award 1751628 from the NSF and under awards R01HL135505 and R21HL139208 from the NIH. **Author contributions:** H.V. and W.W. contributed equally to this work. H.V. and A.K.K. conceived the idea. H.V. and W.W. conducted experiments. H.V. conducted the numerical simulations. H.V., W.W., and A.K.K. conducted analyses. All authors wrote the manuscript. **Competing interests:** The authors declare that they have no competing interests. **Data and materials availability:** All data needed to evaluate the conclusions in the paper are present in the paper and/or the Supplementary Materials. Additional data related to this paper may be requested from the authors.

Submitted 31 May 2018
Accepted 5 October 2018
Published 9 November 2018
10.1126/sciadv.aau3488

Citation: H. Vahabi, W. Wang, J. M. Mabry, A. K. Kota, Coalescence-induced jumping of droplets on superomniphobic surfaces with macrotexture. *Sci. Adv.* **4**, eaau3488 (2018).

Coalescence-induced jumping of droplets on superomniphobic surfaces with macrotexture

Hamed Vahabi, Wei Wang, Joseph M. Mabry and Arun K. Kota

Sci Adv **4** (11), eaau3488.
DOI: 10.1126/sciadv.aau3488